

Heuristic and Eulerian Interface Capturing Approaches for Shallow Water Type Flow and Application to Granular Flows

Hossein Aghakhani, Keith Dalbey, Abani Patra, David Salac

Abstract

Determining the wet-dry boundary and the related spurious thin-layer problem has historically been a challenge when solving the depth-averaged shallow-water (SW) equations (or similar granular flow's equations), and has been the focus of much research effort. In this paper we introduce the use of level set and phase field based methods to solve this issue and related problems. We also propose new heuristic methods to address this problem. We implemented all of these methods in TITAN2D, which is a parallel adaptive mesh refinement toolkit designed for numerical simulation of granular flows. Results of the methods for flow over a simple inclined plane and Colima volcano are used to illustrate the methods. For the inclined plane we verified the results with experimental data and for Colima volcano they have been compared with field data. We successfully captured the interface of the flow and solved the accuracy and stability problems related to the thin layer problem in SW numerical solution. The comparison of results shows that although all of the methods can be used to address this problem, each of them has its own advantages/disadvantages and methods have to be chosen carefully for each problem. **Keywords:** Shallow water flow, Thin layer, Wetting/Drying, Phase field, Level set

1 Introduction

Shallow water (SW) flows include a wide range of fluid flows. In SW flows the fluid depth is much smaller ($\mathcal{O}(10^{-1})$) than the characteristic length of the fluid body. In deriving the corresponding governing equations the shallowness of flow allows us to approximate the variation of state variables in the direction perpendicular to the basal surface and replace them with an integrated average [40], which reduces a three dimension flow into a two-dimensional problem. This approximation holds for many circumstances in geophysical flows and the same conservation equations with some minor variations can be used to study varying physical situations. Eglit and Sveshnikova [22] modified the depth-averaged Saint Venant equations to simulate granular snow avalanches and almost a decade later Savage and Hutter [40] popularized these in the modeling of many geophysical mass flows related to landslides, avalanches and debris flows. Since this type of flow has free moving boundaries one of the basic difficulties of the numerical solution is identifying the location of flow interface. Furthermore, the governing equations are valid only in the wet areas so we need an strategy to discriminate between wet and dry areas in the numerical simulation. In the SW context this is usually called the *wetting and drying (WD)* problem. In our previous work, see Ref. [3], we showed how the speed of waves has to be modified for flow near the vacuum region based on Toro [45] to mitigate the stability problem. However, this still leads to the formation of a non-physical thin layer in the numerical solution, see figure 1 for an illustration. This non-physical thin layer could extend large distances from the realistic main body of the flow, which can cause inaccurate construction of the boundary, loss of conservation or severe numerical instabilities in the numerical solution. Beside the numerical issues, determining probable flow extents through numerical simulation is critical for many SW problems, especially for geophysical flow. For example, in preparing a hazard map for a volcano or a flood it is crucial to know the location of the front of the flow to answer basic questions such as – Does the flow reach a specific location? What is the distance of high risk locations from civil infrastructure? The answer of all the above questions is not possible without good information about the interface of the flow along its flow path. A demonstration of possible issues in

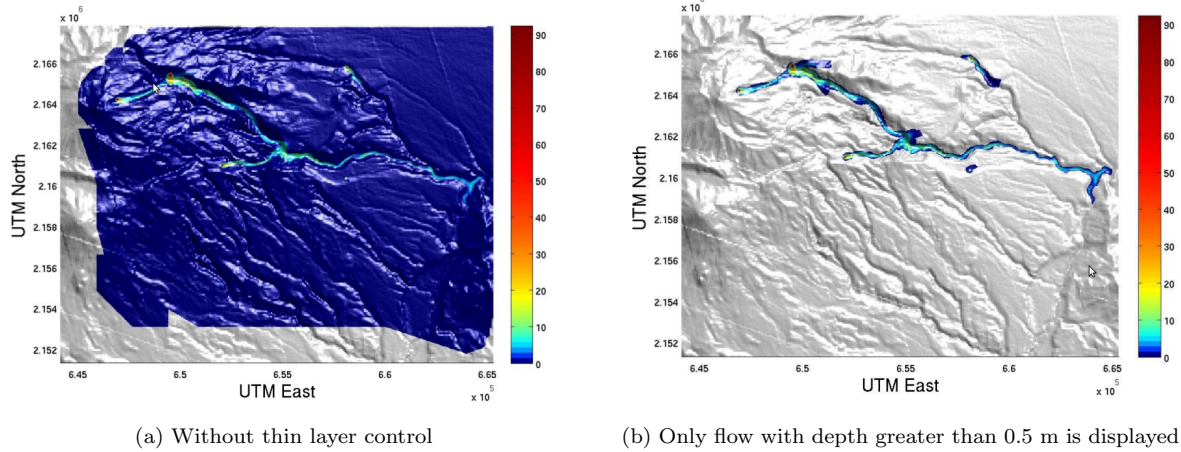


Figure 1: Thin layer problem in maximum over time flow depth simulation of the 1955 debris flow at Atenquique, Mexico [19].

shown in Figure 1. In this figure the numerical simulation of block and ash flows in Atenquique, which is a village near the Colima volcano in Mexico, using a SW like model based on a granular flow assumption is shown. The left figure shows the numerical solution of flow height without using any control for the thin layer problem and the right figure shows the same result using a naive control – plotting the regions with flow height $h > 0.5m$. If no heuristic control on the numerical solution is used the thin layer causes instability and inaccuracy in the obtained results. To summarize, the following major difficulties arise in numerical solutions of SW flows related to the WD or thin layer problem:

1. Ambiguous and subjective computation of flow spreads in SW flows.
2. Unphysically fast estimate of the flow speed. As the solution of SW equations are momentum, $\{hV_x, hV_y\}$, to find velocities, $\{V_x, V_y\}$, used during the solution process the momentum must be divided by flow depth, h , which causes a numerical error if h is small and results in overly large velocities.
3. Unphysical thin layer (orders of magnitude thinner than a grain of sand). This results from the combination of conservation of mass and the numerical wicking away of material.
4. Loss of numerical stability. Due to the above reasons wave-speeds can become infinite at the flow boundary which means that flow equations lose their hyperbolicity at the vacuum state interface.

1.1 Background and Review

A review of the literature shows numerous attempts have been made to overcome these problems [44, 7, 5, 10, 14, 31, 21, 13]. Here we briefly review the problem and recent approaches and refer the interested reader to available references for more information. Generally, all of the approaches can be categorized into two basic groups which we call heuristic methods and interface tracking/capturing methods. The basic idea of heuristic methods is to reconstruct the flow interface based upon some simple heuristic or some algebraic relations. In this approach, the reconstruction could take into account the physics of the problem, but this is not required. For example, to mitigate the thin layer problem a threshold could be defined to control the thin layer, the entire domain could be filled with a shallow level of fluid, the flow could be reconstructed, or the flux could be adjusted. It is possible to use any combination of these heuristic fixes. Most of attempts that are made to address the thin layer problem are categorized under this sort of method [5, 10, 13, 31]. In interface tracking/capturing approaches an auxiliary set of equations is coupled to the original problem. This

auxiliary set of equations is used to follow the flow interface over time. Unlike heuristic method in interface tracking/capturing methods one can find the interface of a moving boundary flow in a more rigorous way. The particular choice of the auxiliary equations leads to either interface tracking, or Lagrangian, methods or interface capturing, or Eulerian, methods. In Lagrangian methods the front is replaced with a set of interfacial points which explicitly define the location of the interface. During each time step these points move due to the numerically computed velocity field. Mark And Cell (MAC) [28], Simplified Mark And Cell (SMAC) [17] and the Surface Marker [49] methods are some examples of Lagrangian interface tracking techniques. The accuracy of the method is highly dependent on the number of particles that form the boundary. High computational cost, a tendency to form numerical instabilities and the inability to track complex topological changes are the most important drawbacks of Lagrangian techniques. For more information about this group of methods please see [25, 47, 36, 4, 29]. In the current paper we focus more on interface capturing or Eulerian methods. In such method the interface is implicitly defined by an additional scalar field defined in the entire computational domain. This additional field is coupled to the other governing equations and evolves due to the underlying fluid flow field. The level set, phase field and Volume of Fluid (VOF) methods are very well-known methods of implicit/Eulerian methods. Hirt and Nichols [29] were the first to propose a VOF method. In this method, the scalar variable is the fraction/volume of a particular fluid in each cell. To construct the interface based on this method an interface surface reconstruction technique is performed at each time step. Youngs [51] achieved a significant improvement in the VOF by adding a piecewise linear interface calculation (PLIC) representation of the fluid boundary. Youngs' method has been shown to be robust and efficient, but it is only first-order accurate. More advanced VOF methods are also available in [24] and Gopala and van Wachem[26], but these method require more complicated logic to reconstruct the interface. The phase field method is an Eulerian interface capturing scheme where the interface is implicitly related to an order parameter which shows the phase variation on the domain [4]. In this method the interface is a diffusive region between phases. The Cahn-Hilliard and Allen-Cahn formulations are two principal formulation for this method [12, 11, 50]. The difference between these two forms is that the first one is mass conservative while the second is not. Mathematically, the conservative form has a forth order derivative while the other one has a second order derivative. This difference in the highest order of derivative will make the later form much easier to implement. Based on our best knowledge no published work has used the phase field method to capture an interface in the shallow water equations. The Level set method is another Eulerian interface capturing technique. It was introduced by Osher and Sethian in 1988 [36]. In this method, the scalar variable is typically a signed distance function which indicates the distance of a grid point to the interface. The only work that used the level set method to mitigate the wetting-drying problem is Quecedo and Pastor [39]. They developed a Taylor-Galerkin approach to solve the SW equations. They presented two different options for handling the wetting-drying areas. The first approach used was described as a “simple yet efficient” method which falls into heuristic method type approaches. Although they claimed that they used level set as the second approach, they did not report any results using the method. They finally concluded that the level set is expensive and unnecessary for their problem.

1.2 Our Contribution

In this paper we describe an approach to the thin layer issue (problems 1-4 discussed in the introduction section), in two parts. The first part is to describe the interface of the flow and the next is to make suitable modifications to meshes, state variables and fluxes based on the result of the first part to resolve the aforementioned issues. To capture the interface we study three different methods. The first one is a new multifaceted Heuristic approach that uses a very small dimensionless threshold, which we call it GEOFLOW-TINY, to distinguish between wet and dry areas. The other methods of interface capturing that we implement are the phase field and level set approaches. To the best of our knowledge the two latter methods are for the first time being applied to geophysical flow. As there are different types of level set and phase field methods available in the literature we initially use the standard level set method and the Allen-Cahn description of the phase field, and modified them as necessary for our problem. The details of implementation of all three methods is explained in related next parts. After finding the interface we make

suitable modifications to address the other issues. In the heuristic approach, after finding the wet and dry cells by using GEOFLOW_TINY, the cells are divided into three groups: wet, dry and partially wet cells. Then we adjust the fluxes for the partially wet cells and then finally update the state variables for wet cells. In the level set and phase field approaches we used the result of these two method for mesh refinement, and by selecting the cells that are close to interface we are able to control the thin layer problem. Details of each approach and how we select the cells for refinement discussed in the relevant section. We verified the numerical results by comparing to experimental results of a granular SW flow over an inclined plane ending in a horizontal surface as well as the field data for the Colima volcano. Results of these tests indicate that the heuristic approach is less expensive than the phase field and level set methods, but the interface using the heuristic method moves faster than the experimentally obtain interface. Additionally, our analysis shows that finding a good threshold that is appropriate for all problems is not easy. On other hand, the interface capturing methods have stronger mathematical and physical structure, and can be coupled with the conservation equations but are computationally more expensive and harder to implement. We used several techniques to decrease the computational cost. For example, in the phase field we used the Allen-Cahn formulation which is easier to implement and computationally less expensive compared to the Cahn-Hilliard formulation, but it is not mass conservative. To preserve the mass we have included a Lagrange multiplier to satisfy this constraint. To decrease the computational cost even more we used operator splitting for time integration. The obtained results show that all of the methods can address the thin layer problem and other related issues, however the phase field results have demonstrated better consistence with the experimental and field data. Finally, although we have implemented these methods for granular type SW flows the methods themselves are applicable for other type of SW flows. The structure of the rest of this paper is as follows. In the next section the shallow-water equations for geophysical flows and the common features of the solver that we used for all of the three methods are introduced. In section 4 the different methods that were employed to mitigate the wetting-drying problem are explained. Discussion and conclusions complete the presentation.

2 Governing Equations

The Savage-Hutter equation for geophysical flows was first introduced in the late 1980's. The original model has subsequently been improved upon by Savage-Hutter themselves as well as others [32, 30, 27, 20, 38, 41]. In our earlier work [37? ?], we developed the Titan2D depth-averaged geophysical flow simulator. Titan2D is a parallel computational tool with dynamic re-partitioning, high order, slope-limiting, upwinding, two-dimensional Godunov solver (without splitting), with adaptive mesh refinement and Geographic Information System (GIS) integration which lets it use Digital Elevation Models (DEMs) of real terrain. While our new multi-faceted thin-layer mitigation strategies were developed in the context of Titan2D's capabilities, much of this approach should be appropriate for use in depth-averaged flow solvers with different numerical implementations. The depth-averaged equations that Titan2D solves are:

$$\begin{aligned} \frac{\partial h}{\partial t} + \frac{\partial(V_x \cdot h)}{\partial x} + \frac{\partial(V_y \cdot h)}{\partial y} &= S_h, \\ \frac{\partial h V_x}{\partial t} + \frac{\partial(V_x \cdot h V_x + 0.5 k_{ap} g_z h^2)}{\partial x} + \frac{\partial(V_y \cdot h V_x)}{\partial y} &= S_x, \\ \frac{\partial h V_y}{\partial t} + \frac{\partial(V_x \cdot h V_y)}{\partial x} + \frac{\partial(V_y \cdot h V_y + 0.5 k_{ap} g_z h^2)}{\partial y} &= S_y. \end{aligned} \quad (1)$$

In these equations:

- The coordinate system (see Figure 2) is aligned such that x and y are directions tangential to the surface of the 3D terrain and z is normal to the surface.
- The effect of terrain elevation is represented by gravitational source terms.
- h is the flow depth in the z direction.

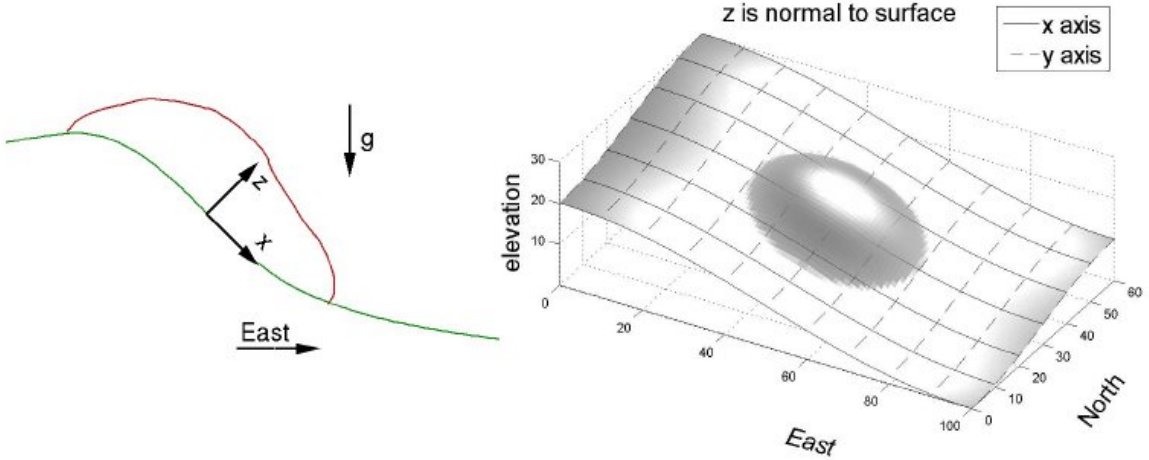


Figure 2: In the local coordinate system the z direction is normal to the surface; the x and y directions are tangential to the surface.

- hV_x and hV_y are the components of “momentum” in x and y directions, respectively.
- k_{ap} is a highly nonlinear term that shows the effect of the earth pressure coefficient, which has active (diverging $\mp = -$), passive (converging $\mp = +$), and neutral (neither diverging, nor converging, $k_{ap} = 1$) conditions:

$$k_{ap} = 2 \frac{1 \mp \sqrt{1 - \cos^2(\phi_{int}) (1 + \tan^2(\phi_{bed}))}}{\cos^2(\phi_{int})} - 1. \quad (2)$$

Note that in the momentum equations $k_{ap}g_z \frac{h}{2}h$ is the contribution of hydrostatic pressure to the momentum fluxes. S_h is a source of mass, i.e. material that either effuses or erodes out of the ground. S_x is the sum of a gravitational driving force, the friction that resists motion of the material relative to the bed, and the friction that resists the internal shearing motion of the material:

$$\begin{aligned} S_x &= g_x h - \frac{V_x}{\sqrt{V_x^2 + V_y^2}} \max \left(g_z + \frac{V_x^2}{r_x}, 0 \right) h \tan(\phi_{bed}) - \operatorname{sgn} \left(\frac{\partial V_x}{\partial y} \right) h k_{ap} \frac{\partial(g_z h)}{\partial y} \sin(\phi_{int}), \\ S_y &= g_y h - \frac{V_y}{\sqrt{V_x^2 + V_y^2}} \max \left(g_z + \frac{V_y^2}{r_y}, 0 \right) h \tan(\phi_{bed}) - \operatorname{sgn} \left(\frac{\partial V_y}{\partial x} \right) h k_{ap} \frac{\partial(g_z h)}{\partial x} \sin(\phi_{int}). \end{aligned} \quad (3)$$

Titan2D solves the above system of equations using a finite volume Godunov method:

$$U_i^{n+1} = U_i^n - \frac{\Delta t}{\Delta x} \{ F_{i+\frac{1}{2}}^n - F_{i-\frac{1}{2}}^n \} - \frac{\Delta t}{\Delta y} \{ G_{i+\frac{1}{2}}^n - G_{i-\frac{1}{2}}^n \}. \quad (4)$$

In the above equation, G and F are the flux terms at the inter-cell boundaries which are computed by the Harten-Lax-Van Leer (HLL) [46] Riemann solver that is explained in the next section.

3 SW Solution and Adaptive Strategy for WD Interface

3.1 Using Appropriate Riemann Fluxes

Following the recommendation of Toro [45], TITAN2D uses the HLL Riemann average of fluxes. Let U be a state variable, F be a flux of that state variable, s be a maximum wave speed, and R and L subscripts which denote “right” and “left” values respectively. The HLL Riemann flux is then

$$F_{HLL} = \begin{cases} F_L & s_L \geq 0 \\ F_R & s_R \leq 0 \\ \frac{s_R F_L - s_L F_R + s_L s_R (U_R - U_L)}{s_R - s_L} & \text{otherwise} \end{cases} \quad (5)$$

For the Savage-Hutter system of equations the characteristic speeds are: $s_{1,3} = v \pm a$ and $s_2 = v$ where v is the velocity of fluid in the corresponding direction and $a = \sqrt{k_{apgh}}$. The above HLL solver is not enough for solving this system of equations. Fraccarollo and Toro [23] note that at the wet-dry boundary the Riemann solution consists of a single rarefaction wave whose speed (when averaged over the cell length) is bounded above by the cell average flow speed plus **twice** the “speed of sound,” $s = v + 2a$, where $a = \sqrt{k_{apgh}}$ for shallow water type granular flows. They also note that “an overestimate of the true wave speeds results in enhanced stability” while an “underestimate of the true wave speeds could be fatal” to stability. They became the first to solve this problem by constructing an approximate Riemann solver.

3.2 Adaptive Meshing

In TITAN2D each grid cell is a square or very nearly so. Rather than using a uniform mesh different sizes of cells are allowed, with each successive “generation” covering one fourth the area of its “parent” cell. Note that only one generation of irregularity is allowed between a cell and its neighbors. At the beginning of the simulation, *i.e.* before the first update, the boundaries of all piles are maximally refined. An initial mesh for a simulation at Colima Volcano, Mexico, is displayed in Figure 3. During normal adaptivity cells are selected

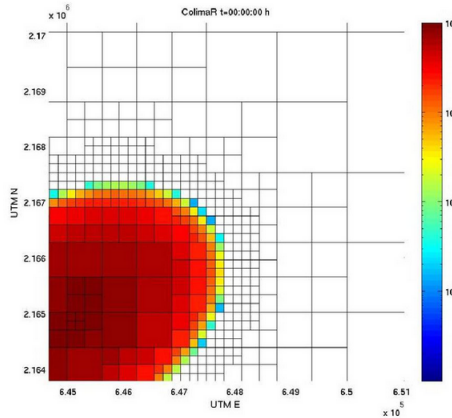


Figure 3: This figure shows four layers of the maximally refined elements near the interface that we call them buffer layer. Creating buffer layers is one of the key strategies that we do to control the thin layer problem in all of the methods that we studied in this work.

for refinement if they meet either of two requirements:

1. They have large, as compared to the average, inter-cellular fluxes.¹
2. They are at or within a few cells near the interface.

The former condition allows for the accurate capture of sharp changes in state variables. The latter results in banded regions of the flow separated into “rings” of maximally refined buffer cells. This limits artificially high transportation of material from the inside of the interface to outside of the interface and guarantees that material will only flow into maximally refined dry cells at the wet-dry front. However, some material that are outside of the recognized boundary may be left outside the outermost band of buffer cells. These cells are not updated until the interface passes them. The rings of buffer cells strategy decreases the numerical wicking problem and when combined with interface capturing scheme it is sufficient to decrease other thin layer problems to a level that prevents the loss of stability. Clearly this strategy depends on the way that we describe the interface. In the heuristic approach, after using a threshold to find the wet and dry areas the number of rings are a number of cells wide equal to or greater than the number of iterations between mesh adaptations (we adapt the mesh after every 5 to 10 time steps). In the level set approach we can use a narrow band method for adaption and selecting of these buffer rings, but we simply select the elements such that their distance to the interface are less than a normalized distance that is obtained from the maximum distance to the interface. Note that in the level set method distance of the cells to the interface is the level set function itself and we do not pay any additional computational cost for that information. In the phase field method we have a diffusive region between two phases that we can control with a capillary width (please refer to section 4.2). We are thus able to select those cells such that $|\phi| < 1$ where ϕ the phase field value. We set the capillary width equal to the number of time steps between successive adaptivity steps. Unrefinement takes place immediately after refinement; a group of four “sibling” cells will be selected to merge into their mutual “parent” cell if the sum of their inter-cellular fluxes is very low compared to the average flux. Cells that have either just been refined or are otherwise in any of the current bands of buffer cells are immune to unrefinement.

4 Interface Capturing Strategies

In the aforementioned parts the major difficulties of numerical analysis of the shallow water equations were discussed, and it was shown that most of them are directly or indirectly related to the WD problem. For more intuition, the result of a simulation for Atenquique debris is displayed in figure 1. The left picture is the obtained result from the solver and the right picture is the same result, but flow height is displayed only for flow height greater than 0.5 m. This picture shows for the pure solver the dominant part of the domain is filled with negligible flow depth and this makes the actual interface mix with the thin layer region. In this section three methods to solve the WD problem which mitigate the numerical difficulties of SWE are explained.

4.1 First: Heuristic methods

Usually, heuristic methods use one or a combination of the following four strategies [44]:

1. Filling the entire computational domain with a thin layer of fluid,
2. Using a depth scale to check whether a cell or a node is wet or dry (or possibly partially wet), and then making a decision to add or remove it from the computational domain,
3. Employing some extrapolating scheme from the wet cells into their neighbor cells to approximate the location of the interface. This method is usually called volume/free-surface relationship (VFR) in the literature,

¹More systematic error estimate driven approaches have been tried [THIS NEEDS A CITATION](#) but empirical experience suggests that these simple indicators provide sufficient information for reliable and fast simulations.

4. Permitting fluid height to be negative, which means that it is below the topographical surface.

Table 4.1 compares these heuristic methods.

Strategy	Mass Conservation	Physics
Thin film	Adequate, but requires solution reconstruction	Produces a smooth and realistic wetting front
Cell removal	Dependent on numerical method for solving the equations	Excellent, performs better on advancing front than receding front
VFR	Conservative, with aid of some correction procedure	Very good in wide verity of problems
Allowable negative depth	Conservative, but performance depend on WD parameters	Same as mass conservation

The heuristic method that we used in this study can be categorized as a VFR method. That its detail is explained the related part.

4.1.1 Selecting appropriate threshold

In this approach we use a very small threshold for flow height to segregate the wet, partially wet and dry cells. The critical contribution of this scaling is to allow other facets like flux adjustment and boundary reconstruction to identify where the flow is non-physically thin, *i.e.* where should they consider the boundary of the flow to be. Consistency is the key requirement of whatever strategy we choose to determine the scaling. That is, the chosen strategy must be able to generate the same “appropriate” value for depth scale at the beginning and at the end of a simulation. In a “typical” geological simulation, say of the collapse of a volcanic dome which would be modeled in TITAN2D as a “pile source”, the initial body of mass can be quite deep, but at the end of the simulation the material will likely be spread over a large area. Hypothetically, if one were to scale by maximum flow depth at the beginning and end of the simulation, they would obtain vastly different values. More importantly, if the only source of mass was an effusion of material out of the ground, the maximum initial flow depth would be zero, even if the total volume during the course of the simulation was the same as the previously mentioned “pile source”. On the other hand, scaling by the cube root of the total volume of the flow being simulated is entirely consistent and is the flow depth scaling factor used by TITAN2D. We do **not** claim that the cube root of volume is any more or less appropriate as a scaling factor than maximum initial flow depth in other shallow water contexts, for example storm surge simulation. Having chosen a consistent scaling factor we were then able to define associated non-dimensional depths for negligibly thin and merely thin flows. If one were to assume that a particular geophysical mass flow event involved a volume of $10^8[\text{m}^3]$, it would then be reasonable to state that flow depths of less than $5[\text{cm}]$ were both negligible and non-threatening. This roughly equates to non-dimensional negligible flow depth, which we call **GEOFLOW_TINY**, with the value

$$\text{GEOFLOW_TINY} = 0.0001. \quad (6)$$

Using this value, and assuming the volume used in a laboratory scale test was $1[\text{cm}^3]$, the resultant negligible flow depth would be $0.0001[\text{cm}]$. As can be observed from these two examples, the chosen value of **GEOFLOW_TINY** is physically appropriate across a very large range of volumes. We therefore use a theoretical contour at this depth as the boundary of the simulated flow. In the introduction section we stated that unless steps are taken to prevent it, the numerical wicking (Problem 2) will cause the flow to spread 1 cell every time-step even though the product of flow speed and time-step size is less than the cell length. In addition, the familiar continuum equations loose hyperbolicity (wave speeds tend to infinity) at the boundary between a continuous material and a vacuum. Having implicitly defined the flow boundary, we prevent calculation of state variables outside the flow, *i.e.* in regions with flow depth below **GEOFLOW_TINY**. This reduces both non-physical flow spreading and computational cost. Note that state variables in cells with flow depth less than **GEOFLOW_TINY** are **not** zeroed.

4.1.2 Interface Reconstruction

As noted above, the use of a standard Eulerian grid imposes discrete fixed increments to the flow extent which contributes to the wicking problem (Problem 2) at the boundary. Use of adaptive mesh refinement reduces this error by reducing the amount of the increment. The Lagrangian approach does not have this limitation, which Tai et al. [43] took advantage of when they augmented their one dimensional NOC scheme with Lagrangian front tracking. However, implementing a hybrid Eulerian-Lagrangian scheme in two dimensions is significantly more complex. Therefore, as part of our multi-faceted approach we implemented a very simple and inexpensive interface reconstruction and predictive Lagrangian front tracking scheme. Knowledge of the interface allows us to generate a representative average for an individual cell edge over the time-step and for values of state variables which are then used to compute inter-cellular fluxes into/out-of partially wet cells. The interface reconstruction scheme is illustrated in figure 4. Specifically, each partially wet cell is assumed

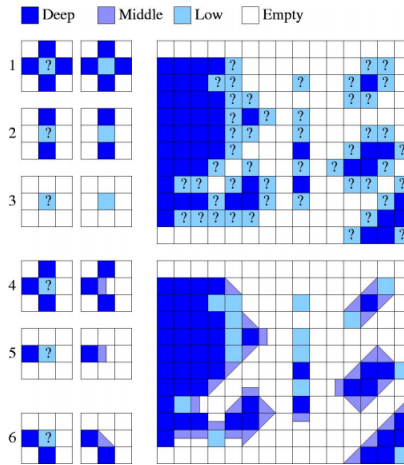


Figure 4: Interface Reconstruction in TITAN2D

to be split by a straight line into a completely dry and a completely wet part. For the sake of simplicity, we restrict this line to one of four orientations: east-west, north-south, or parallel to either diagonal of the square cell. However, all placements/translations of the wet-dry line are allowed. At the beginning of each time-step, the orientation of the line for the entire time-step is set based solely on which of the cell's neighbors have flow depth greater/less than the `GEOFLOW_TINY` threshold². Orientation of the wet-dry line, and which side of it is wet, is indicated by a single integer representing the geometrically determined “most wet node.” The only nine possible values for the most wet node are any of the cell’s corners, edge midpoints or its center. The most wet node is assumed to have a flow depth that is the maximum of the cell or any of its four neighbors. The placement of the line is such that the volume of material in the cell under a plane passing through the most wet node and the wet dry-line is the same as the unadjusted cell. Since we now know where the wet-dry line is at the beginning of the time step, we can compute which of the cell’s edges are completely wet, completely dry, or partially wet, and the fraction of wetness for the partially wet edges. Given the orientation and beginning of time-step location of the wet-dry line and the cell’s state variables, it is also fairly straight forward to predict the line’s end of time-step location. This is done by convecting the wet-dry line at the shock speed, $s = v + a$ where the speed of sound has been adjusted to account for only part of the cell being wet, i.e. $a = \sqrt{k_{ap}gh \frac{A}{A_{wet}}}$. Here A is the whole cell’s area and A_{wet} is the portion of the cell’s area that is wet. Since the wet-dry boundary within each partially wet cell is assumed to be a straight line with, during the time-step, fixed orientation, convecting a single point, in this case the midpoint, on the

²As stated in Subsection 3.2, the refinement strategy ensures that the flow front will always be maximally refined. This simplifies the coding since all cells at the front can be safely assumed to have only one neighbor on each side.

line is equivalent to convecting the entire wet-dry line. A spatial and time average of the wetness factor for the edge over the time-step can therefore be easily computed as

$$W = \left(\frac{0 \cdot \Delta t_{dry} + \frac{1}{2}(w_{beg} + w_{end})\Delta t_{part} + 1 \cdot \Delta t_{wet}}{\Delta t} \right) \left(\frac{A}{A_{wet}} \right) \quad (7)$$

where $\Delta t = \Delta t_{dry} + \Delta t_{part} + \Delta t_{wet}$ is the entire time-step, Δt_{dry} is the portion of the time-step for which the edge is completely dry, Δt_{part} is the portion of the time-step for which the edge is partially wet and partially dry, Δt_{wet} is the portion of the time-step for which the edge is completely wet, w_{beg} is the edge's fraction of wetness at the beginning of the time-step, and w_{end} is the edge's fraction of wetness at the end of the time-step.

4.1.3 Adjusting Fluxes in Partially Wet Cells

The state variables used to compute the physical fluxes are the whole cell average values multiplied by the edge wetness factor. Note this results in the zeroing of this cell's physical fluxes for its sides that will be completely dry for the entire time-step and increasing them for sides that will be completely wet for the entire time-step. The numerical fluxes are then taken to be the HLL Riemann average of the "adjusted" physical fluxes from the cells on both sides the edge. The wetness factor adjustment of fluxes delays/decreases the transfer of material from partially wet cells to completely dry cells. This delay significantly reduces the amount of non-physical flow spreading, and requires negligible additional computation and memory usage. In terms of memory usage, this scheme only requires one additional integer indicating the most wet node, and two additional decimal numbers for the cell's fraction of wet area and the location of the wet-dry line's midpoint (implemented as a single number ranging from zero to one). The flux adjustment in partially wet cells mitigates the numerical wicking (Problem 2) at the boundary but not within the flow (that requires either a uniform grid or an adaptive strategy based on fluxes and the rings of buffer cells strategy).

4.2 Second: Phase Field Method

As noted earlier, another approach that is employed for capturing the interface of a SW type flow is the phase field method. In this method the state variables are augmented by a continuous order parameter. This order parameter, φ , implicitly represents the interface in the domain. To this aim, a new transfer equation must be solved which is coupled with the other state variables. Papers [16, 4, 8, 33] are good references about the history and evolution of the method. Phase diffusion methods and particularly the phase field method is based upon the notion that the interface between phases is a diffusive region rather than a sharp interface. The value of ϕ is constant within a bulk phase but changes smoothly between the phases. In this work ϕ is 1 for the fluid phase $\{\mathbf{x} : \phi(\mathbf{x}, t) = 1\}$, and it is -1 for void regions $\{\mathbf{x} : \phi(\mathbf{x}, t) = -1\}$, and is between -1 to 1 on the diffusion region $\{\mathbf{x} : -1 < \phi(\mathbf{x}, t) < 1\}$. We can implicitly assume the interface of the flow is where $\{\mathbf{x} : \phi(\mathbf{x}, t) = 0\}$. In this study we used Allen-Cahn form of the phase field.

$$\frac{\partial \varphi}{\partial t} + \vec{V} \cdot \nabla \varphi = \gamma(\Delta \varphi - F'(\varphi)), \quad (8)$$

where

$$F(\varphi) = \frac{1}{4\eta^2}(\varphi^2 - 1)^2, \text{ so } F'(\varphi) = \frac{\delta F}{\delta \varphi} = \frac{1}{\eta^2}\varphi(\varphi^2 - 1). \quad (9)$$

In above equation η is a constant that regulates the capillary width or diffusion width, and γ denotes an elastic relaxation constant, and $F(\varphi)$ is a mixing free energy which is the well-known double-well potential function, and represents the interactions of different volume fractions of individual species [9, 34]. This formulation is easier to solve, but is not mass conservative, to conserve the mass a Lagrange multiplier in form of $(\varphi^2 - 1)\xi(t)$ is added as a source term to the right hand side of equation (8). The reason that we

select this form for the Lagrange multiplier is because we do not want to change φ on the bulk region as well as when on the interface i.e when $\varphi = \pm 1$. So the final form of equation $\xi(t)$ would be:

$$\frac{\partial \varphi}{\partial t} + \vec{V} \cdot \nabla \varphi = \gamma(\Delta \varphi - F'(\varphi) + (\varphi^2 - 1)\xi(t)), \quad (10)$$

and the constrain that has to be satisfied is:

$$\frac{D}{Dt} \int_{\Omega} \varphi h \, dx = 0, \quad (11)$$

which basically means the initial volume of pile must be constant during the simulation. Consequently $\xi(t)$ is derived as follow:

$$\frac{D}{Dt} \int_{\Omega} \varphi h \, dx = h \int_{\Omega} \frac{D}{Dt} \varphi \, dx + \underbrace{\varphi \int_{\Omega} \frac{D}{Dt} h \, dx}_{=0 \text{ continuity}} = h \int_{\Omega} \gamma(\Delta \varphi - F'(\varphi) + \varphi(\varphi^2 - 1)\xi(t)) \, dx, \quad (12)$$

the first term in above relation will be neglected by applying the Gauss' theorem with considering the boundary conditions ($\frac{\partial \varphi}{\partial n}|_{\Gamma} = 0$,):

$$\int_{\Omega} h \gamma \nabla \cdot \nabla \varphi \, dx = \int_{\Gamma} h \gamma \nabla \varphi \cdot \hat{n} \, ds = 0, \quad (13)$$

so to always satisfy the constrain (11) we end up with:

$$\frac{1}{\eta^2} \int_{\Omega} \varphi(\varphi^2 - 1) \, dx = \xi(t) \int_{\Omega} (\varphi^2 - 1) \, dx \Rightarrow \xi(t) = \frac{\int_{\Omega} \varphi(\varphi^2 - 1) \, dx}{\eta^2 \int_{\Omega} (\varphi^2 - 1) \, dx} \quad (14)$$

We set $\eta = n \delta x$, where δx is equal to the smallest cell length of all elements and n is the number of the buffer layers explained in section 3.2. Form time integration of equation (10) we use operator splitting to get benefit of proper scheme for each part of the equation. We use the Euler explicit method for time integration of all terms except the Laplacian terms, and update the Laplacian term by the Euler implicit scheme. The length of time step is based on CFL condition for the explicit scheme.

$$\frac{\varphi^{i+5} - \varphi^i}{\Delta t} = \gamma(-F'(\varphi^i) + \varphi^i(1 - (\varphi^i)^2)\xi(t^i)) \quad (15)$$

$$\frac{\varphi^{i+1} - \varphi^{i+5}}{\Delta t} = \gamma \nabla \cdot \nabla \varphi^{i+1} \quad (16)$$

We used GMRES solver of the PETSc [6] library to solve equation (16). Since the Krylov subspace solvers just needs the result of matrix-vector multiplication, we used matrix-free method to compute the laplacian term to decrease the memory cost of implicit solver.

4.3 Third: Level Set Method

The last method that we use to capture the interface for a SW flow is the Level set method. The Level set method is another Eulerian interface capturing method; it was introduced by Osher and Sethian in 1988 [36]. The basis of the method is to capture the interface by means of solving a hyperbolic Hamilton-Jacobi PDE on the computational domain which follows the boundaries. The level set variable $\Psi(X, t)$ implicitly represents the interface. In this method, $\Psi(X, t)$ is a signed distance function which means it is zero on the interface, and its absolute value changes in the domain with respect to the distance to the zero level, and its sign is positive outside of the interface, and is negative inside of the interface. Given the initial condition $\Psi(X, t)_0$ the advection of the interface ($\Psi(X, t) = 0$) only depends on the normal velocity F :

$$\frac{\partial \Psi}{\partial t} + F |\nabla \Psi| = 0, \quad (17)$$

substituting $F = \vec{V} \vec{n}$ which \vec{n} is the normal vector, and is equal to $\frac{\nabla \Psi}{|\nabla \Psi|}$ leads to:

$$\frac{\partial \Psi}{\partial t} + \vec{V} \nabla \Psi = 0 \quad (18)$$

4.3.1 Reinitialization

Solution of equation (18) is not essentially a signed distance function, to keep Ψ a signed distance function, we need a procedure that is called initialization or reinitialization. There are several techniques for this purpose [36], but what we implemented here is a composition of the method presented in Chopp's work [18] with some modifications, for the points close to the interface, and a PDE based initialization for the further places[42]. PDE based initialization is easy for parallelization, though it suffers from preserving the interface location that causes loose of conservation mass/area. Chopp's suggests a bicubic interpolation for the points near the interface [18], but here we use a bilinear interpolation which is not as accurate as what he suggested, but it is accurate enough to preserve the interface. For further distances we do not need very accurate Ψ , so we use a PDE based reinitialization which is easier to implement and has lower computational cost. In our approach, we first find Ψ for the points that are adjacent to the interface, then use these points to update the signed distance function for rest of the points by PDE based initialization. In this way, the interface ($\Psi = 0$) is preserved with an affordable computational cost and effort. Moreover, since just Ψ is required for the points that are located near the interface, there is no need to update it for whole of the domain, so in this work we select $\Psi_{thresh} < 10 \delta x$, which δx is the smallest size of the elements, as the threshold for updating Ψ in the initialization. The signed distance function is updated for adjacent points to the interface in following steps:

1. First we find the adjacent points to the interface, and store them in a list that is usually called accepted points list in the literature [18].
2. Second step is to find an interpolation for a level set function $p(X)$ that returns $\Psi(X)$ given the position of the points.
3. The last step is to compute the distance of accepted points based on the following conditions:

$$p(X_{int}) = 0, \quad (19a)$$

$$\nabla p(y) \times (X_0 - X_{int}) = 0, \quad (19b)$$

where X_{int} is the nearest point on the interface, and X_0 is the point in the accepted list that we want to compute its distance to the interface. First condition (19a) basically means that X_{int} is on the interface, and the second condition says that if we draw a line from X_0 to closest point on the interface, it has to be perpendicular on intersection point with the interface. In this part, we followed the notation of Chopp's paper [18].

In the first step, we just need to find those points that sign of Ψ is different from their neighbors, and store them in a list that we call them accepted points list. For the second step, there are different ways for interpolation through the accepted points and finding p . In many applications, like in this study, initial interface has a specific geometrical shape like circle or ellipse, so we do not need to find it approximately, and its equation can be used directly as $p(X)$. For example, in this study initial pile has elliptic shape, so the initial interface follows elliptic equation. If we do not know the equation of the interface which is usually the case, especially in the reinitialization, we need to find p by interpolation. Chopp's suggested a bicubic approximation [18] to achieve a fully second order accurate result, but his method yields to solve a 16 by 16 system of equations for every four neighbor points in the accepted list to find the coefficient of the bicubic interpolation. Since the whole point of this interpolation is to compute the distance to the interface more accurately, in order to preserve the location of the interface, in this study instead of bicubic approximation we used a bilinear interpolation. So the general form of p is:

$$p = a_0 + a_1 x + a_2 y + a_3 xy. \quad (20)$$

A general way to find a_0 to a_3 for a grid with different element sizes is to solve a system of 4 by 4 equations (21) resulted from value of Ψ and the positions of the points.

$$\begin{bmatrix} 1 & x_1 & y_1 & x_1y_1 \\ 1 & x_2 & y_2 & x_2y_2 \\ 1 & x_3 & y_3 & x_3y_3 \\ 1 & x_4 & y_4 & x_4y_4 \end{bmatrix} \begin{bmatrix} a_0 \\ a_1 \\ a_2 \\ a_3 \end{bmatrix} = \begin{bmatrix} \Psi_1 \\ \Psi_2 \\ \Psi_3 \\ \Psi_4 \end{bmatrix} \quad (21)$$

But since here we maximally refine the elements near the interface, all of the elements that are selected for the interpolation have the same size and four cell centers can be considered as the vertices of a rectangle, so the coefficients of equation (20) can be computed as following:

$$a_0 = \frac{(\Psi_1x_2y_2 - \Psi_2x_2y_1 - \Psi_3x_1y_2 + \Psi_4x_1y_1)}{(x_2 - x_1)(y_2 - y_1)}, \quad (22a)$$

$$a_1 = \frac{(-\Psi_1y_2 + \Psi_2y_1 + \Psi_3y_2 - \Psi_4y_1)}{(x_2 - x_1)(y_2 - y_1)}, \quad (22b)$$

$$a_2 = \frac{(-\Psi_1x_2 + \Psi_2x_2 + \Psi_3x_1 - \Psi_4x_1)}{(x_2 - x_1)(y_2 - y_1)}, \quad (22c)$$

$$a_4 = \frac{(\Psi_1 - \Psi_2 - \Psi_3 + \Psi_4)}{(x_2 - x_1)(y_2 - y_1)}, \quad (22d)$$

$$(22e)$$

where $\Psi_1 = (x_1, y_1)$, $\Psi_2 = (x_1, y_2)$, $\Psi_3 = (x_2, y_1)$ and $\Psi_4 = (x_2, y_2)$ as can be seen in the figure 5. After finding

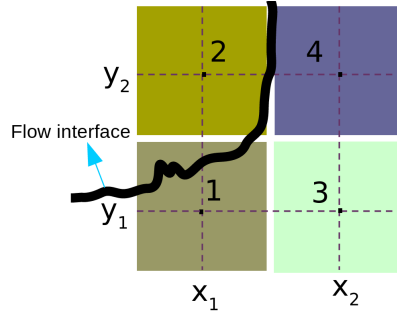


Figure 5: Configuration of the four elements that have been selected for bilinear interpolation. In this schematic example the interface passes through two hypothetical edges of (2-4) and (1-2) edges. This is just for demonstration purpose and has no effect on the equations.

the interpolation p , we can compute the distance from equation (19a) and (19b). These equations form a nonlinear system of equations that we use a variant of Newton's method presented in [18] to solve them:

$$\delta_1 = -p(X^k) \frac{\nabla p(X^k)}{\nabla p(X^k) \cdot \nabla p(X^k)}, \quad (23a)$$

$$X_{1+\frac{1}{2}} = X_k + \delta_1, \quad (23b)$$

$$\delta_2 = (X^0 - X^k) - \frac{(X^0 - X^k) \cdot \nabla p(X^k)}{\nabla p(X^k) \cdot \nabla p(X^k)} \nabla p(X^k), \quad (23c)$$

$$X_{k+1} = X_{1+\frac{1}{2}} + \delta_2, \quad (23d)$$

equation (23) is an iterative method that starts from X_0 which is the point that we want to find its distance to the interface. Clearly, above equation gives the nearest point on the interface, and then the distance can

be computed, and sign of Ψ is same as what it was before reinitialization. For interpolation in (20), we need four points. When we create accepted list, instead of storing points we store a pair of points that are neighbor and their sign of Ψ is different. Then to find two other points, it is enough to select a direction perpendicular to the direction that connects the selected pair, and find the neighbors of the first two points in this direction. Before proceeding to the next step about PDE based initialization that we use for the rest of the points, we like to mention some computational remarks about the aforementioned step. In parallel computation we decompose the domain between the processors, and each processor is responsible for a part of the domain. On other hand, in finite volume we need the information of the neighboring cells to compute the fluxes and the derivatives. For those elements that are on the boundary of the decomposed parts these information are living in the other processors, so to have this information one solution that avoids excessive inter-processor communications is to make a copy of these off-processors cells on the other processor that we need their information to update the cells. This group of cells that are updated in the other cells, but we need their information in another processor are called ghost cells. Depend on the stencil that is used in computing the derivatives and fluxes different layers of the ghost cells are required. For example for a five point stencel we need the information of neighbor and neighbor of neighbor cells, and in TITAN2D, we just need the neighbor information. We mentioned this here because in selecting the points for interpolation, we have the information of the neighbor cells, but as described earlier, we also need the information of neighbor of a neighbor for the interpolation. This case is a challenge when the interface exactly passes on the decomposition boundary which means a cell that is inside of the flow has a neighbor ghost cell which is outside of the boundary. Compare to the number of accepted cells that is a rare case, and so to avoid the communication to get the information of the neighbor of neighbor ghost cell we find the interpolation here in a different way. For this cases, instead of using a bilinear interpolation we use three points to make a surface and do the interpolation in form of (24):

$$p = a_0 + a_1x + a_2y \quad (24)$$

Two of these three points are coming from the pair that we know the interface is passing through them and previously have been stored in the accepted list, and the third point is of the the neighbors that we have its information which is perpendicular to the hypothetical edge that connects the selected pair (figure 6). Having these three points we first make two vectors and then the normal vector to these two vectors which is the normal vector of the surface. With the normal vector and one of the points we can find the p equation which satisfies the three points as follow:

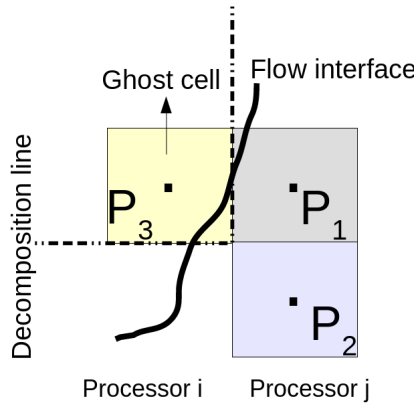


Figure 6: In this figure p_1 and p_2 are updated in processor j and p_3 is updated in processor i, but its information is available in processor j as ghost cell.

$$p_1 = \begin{bmatrix} x_1 \\ y_1 \\ \Psi_1 \end{bmatrix}, \quad p_2 = \begin{bmatrix} x_2 \\ y_2 \\ \Psi_2 \end{bmatrix}, \quad p_3 = \begin{bmatrix} x_3 \\ y_3 \\ \Psi_3 \end{bmatrix},$$

$$\vec{n} = \overrightarrow{p_2 p_1} \times \overrightarrow{p_3 p_1} = \begin{bmatrix} n_1 \\ n_2 \\ n_3 \end{bmatrix} = \begin{bmatrix} (y_2 - y_1)(\Psi_3 - \Psi_1) - (y_3 - y_1)(\Psi_2 - \Psi_1) \\ (x_3 - x_1)(\Psi_2 - \Psi_1) - (x_2 - x_1)(\Psi_3 - \Psi_1) \\ (x_2 - x_1)(y_3 - y_1) - (x_3 - x_1)(y_2 - y_1) \end{bmatrix}, \quad (25)$$

$$a_0 = \frac{n_1}{n_3} x_1 + \frac{n_2}{n_3} y_1 + \Psi_1 \quad a_1 = \frac{-n_1}{n_3}, \quad a_2 = \frac{-n_2}{n_3} \quad (26)$$

Another point that we want to make here is that our experience shows using set container of C++ standard library is a very proper data structure for storing the adjacent points near the interface in the first step. The reason is that this container keeps its item in a sorted way, and does not let to store duplicated items. So when we search to find those neighbors that have different Ψ signs to store them in the list, we will not worry to store an element more than once, and there is no need to check the list every time that we want to save a new element to make sure that we have not saved it before. Only thing that one has to do is to overload the less operator by the desired properties of the elements, that could be element's position or key, to have a sorted list with the unique items. After finding Ψ for the points adjacent to the interface, Ψ in other points can be updated with a PDE based reinitialization in an unwinding scheme. We used the following PDE for this aim:

$$\frac{\partial \Psi}{\partial \tau} + \text{sgn}(\Psi_0)(|\nabla \Psi| - 1) = 0 \quad (27)$$

In equation (27) τ is a pseudo-time and the equation should be solved until it converges reasonably. This PDE adjusts Ψ such that $|\nabla \Psi| = 1$. We solve equation (27) by the method introduced in [2].

$$\Psi_{ijk}^{n+1} = \Psi_{ijk}^n - \Delta t \left(\max(F, 0) \nabla_{ijk}^+ + \min(F, 0) \nabla_{ijk}^- \right), \quad (28)$$

where

$$\nabla_{ijk}^+ = \left[\max(D^{-x}\Psi_{ijk}^n)^2 + \min(D^{+x}\Psi_{ijk}^n)^2 \right. \\ \left. \max(D^{-y}\Psi_{ijk}^n)^2 + \min(D^{+y}\Psi_{ijk}^n)^2 \right]^{1/2} \quad (29)$$

$$\nabla_{ijk}^- = \left[\min(D^{-x}\Psi_{ijk}^n)^2 + \max(D^{+x}\Psi_{ijk}^n)^2 \right. \\ \left. \min(D^{-y}\Psi_{ijk}^n)^2 + \max(D^{+y}\Psi_{ijk}^n)^2 \right]^{1/2} \quad (30)$$

In the above equations D^+ , and D^- are respectively the backward and forward differences in the corresponding directions. We solve equation (27) until we reach the convergence or make sure that we have updated the points far enough from the interface. The threshold that we used for convergence was $.5(\delta x)^3$.

5 Results

We use two cases to study the effects of the introduced interface capturing schemes in the section. The first case is the inclined plane, and the second one is the Colima Volcano. The reason that we selected these two cases is that for the inclined plane we have conducted experimental test, so the numerical study results could be verified with the experimental results. For the later one, i.e Colima Volcano, we used the field observation data of the outline and characteristic of the flow to simulate an eruption numerically and compare the results.

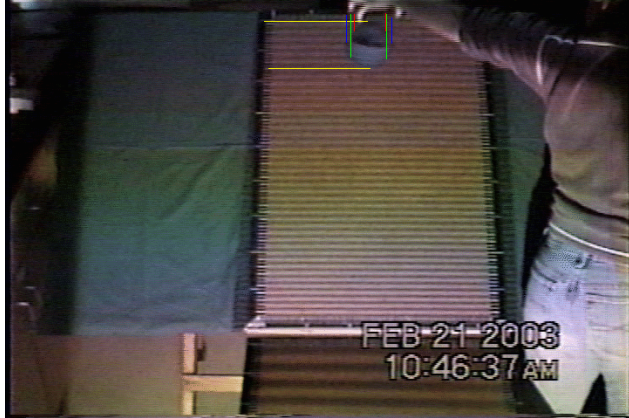
Since the computational cost of the methods are not same, we have also compared these methods from computational point of view by the required time for simulation and the number of elements during the simulation.

5.1 Inclined plane

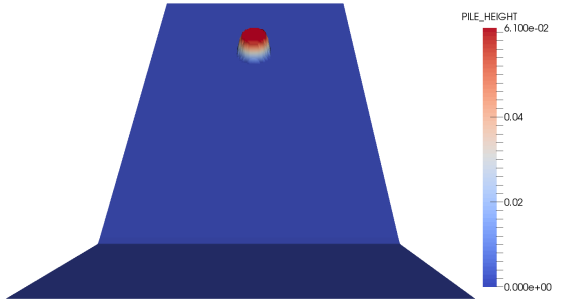
In this section the results of the inclined plane is presented. The input parameters and initial conditions of the flow could be seen in table 1.

Pile shape	Cylindrical
Maximum pile height	.061 m
Major extent of the pile	.0525 m
Minor extent of the pile	.0525 m
Bed friction angle	32.47°
Internal friction angle	37.3°
Angle of incline	38.5°
Physical time simulated	90 sec

The experimental test results were reported in [48], and we have used them to verify our different numerical results with them in our previous works.



(a) Experimental setup



(b) Numerical simulation

Figure 7: Initial configuration of the pile on the incline

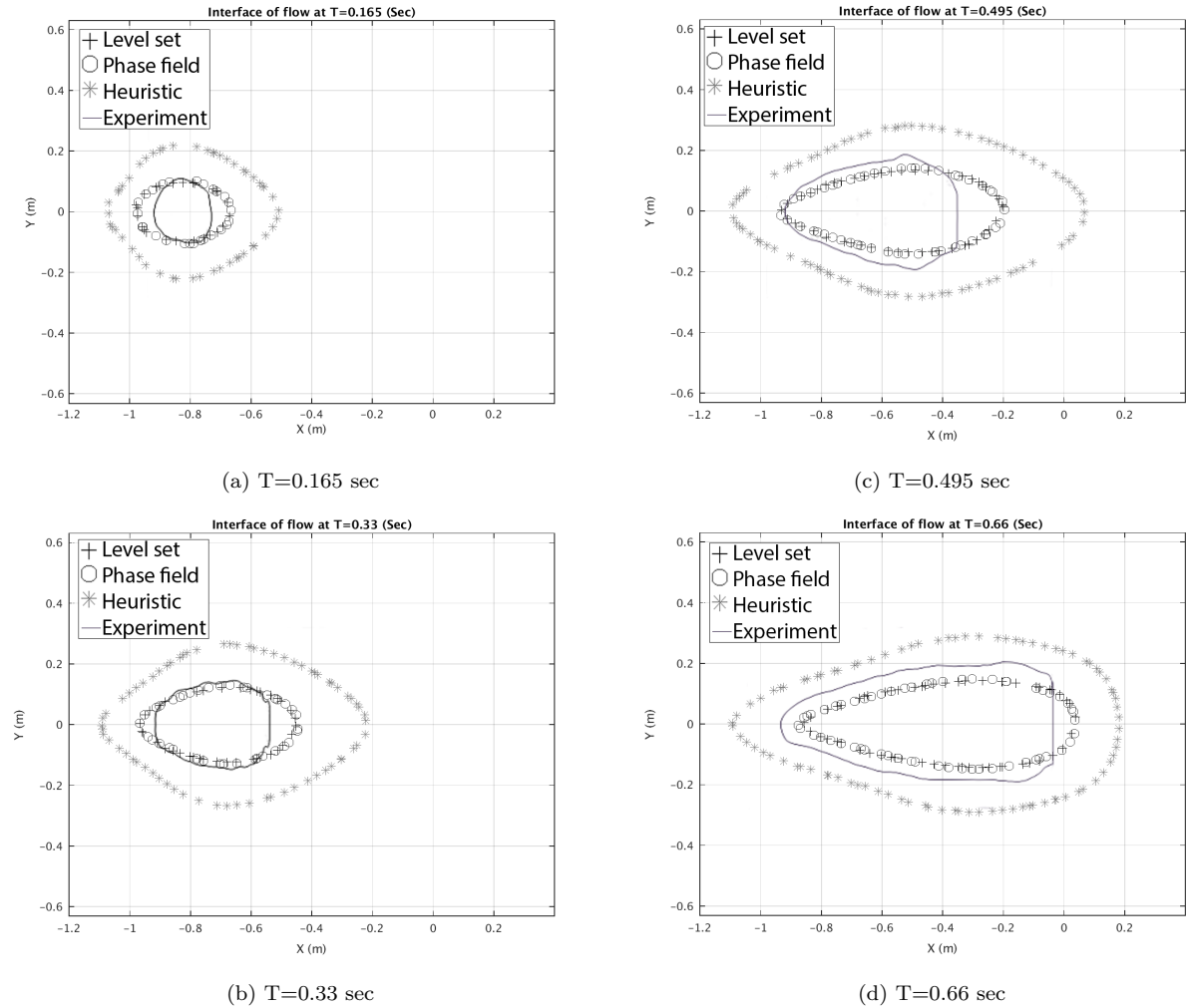


Figure 8: Pile height contour and interface location at different time steps

5.1.1 Comparison

For quantitative comparison of the results, we compared different schemes on three measurable quantities. The first measure is the extent of pile in X direction, the second one the extent of pile in Y direction, and the last one is the area of pile.

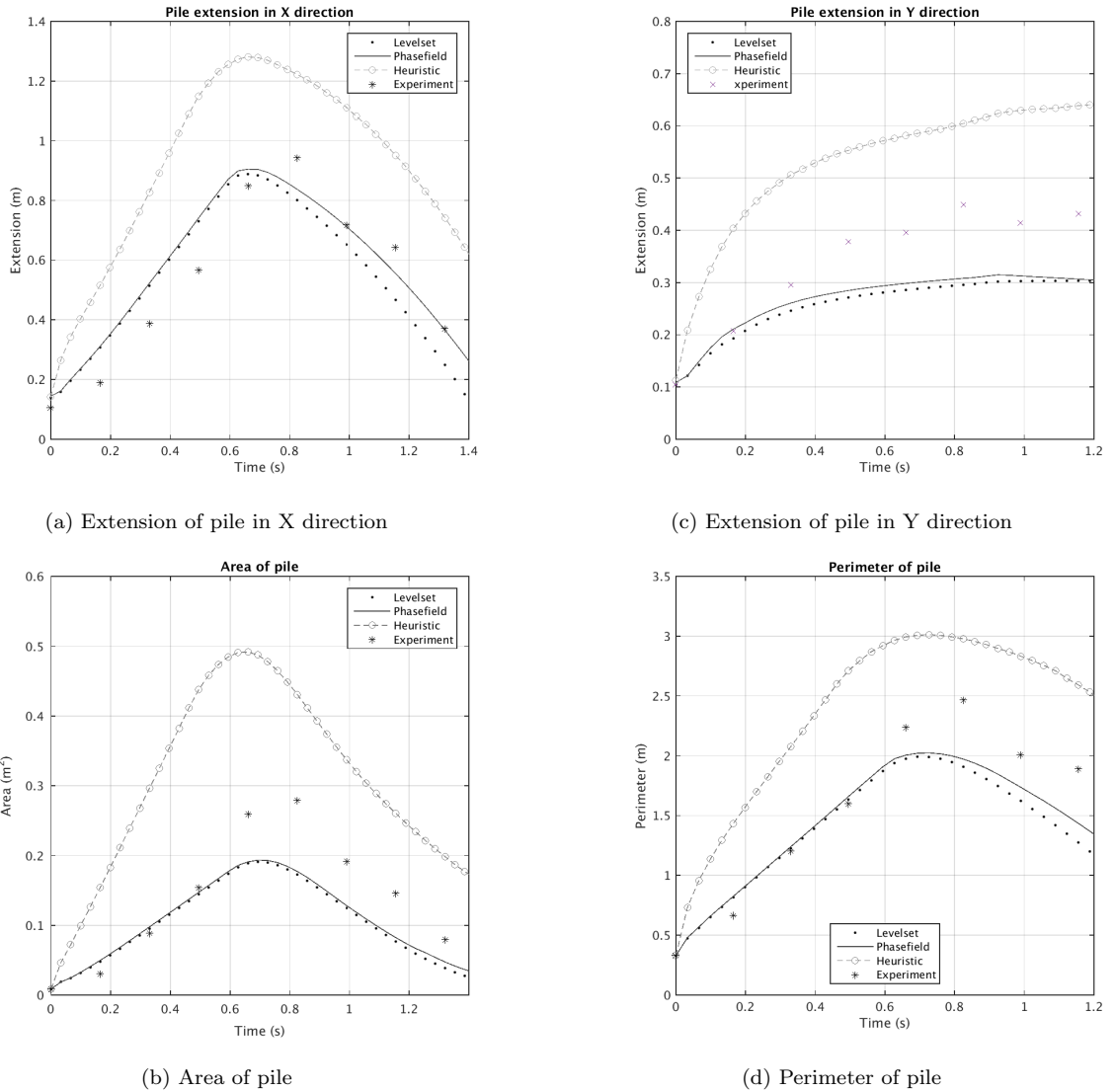
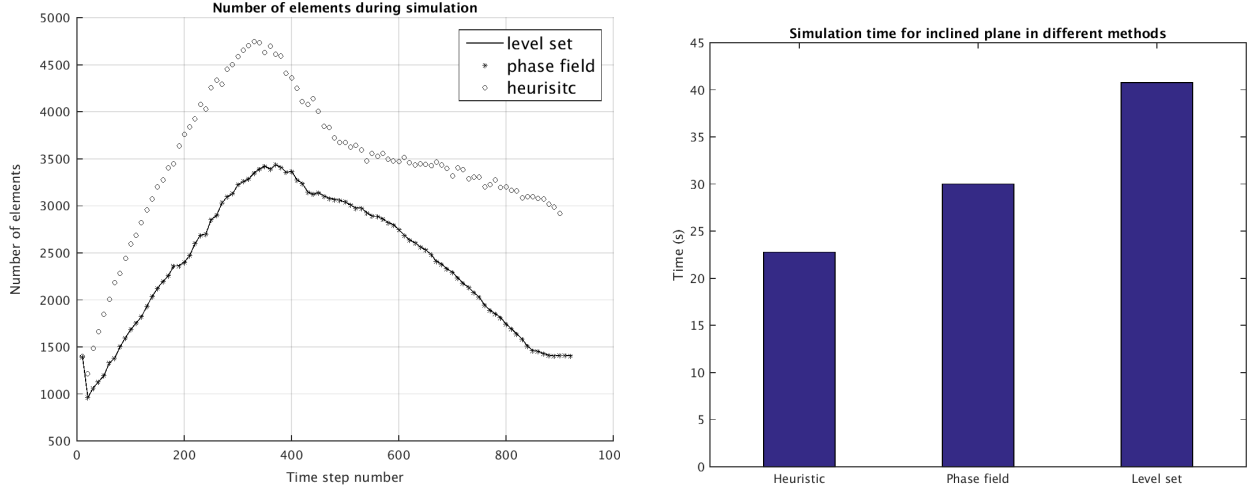


Figure 9: Comparison of the methods for flow on inclined plane



(a) Number of the elements for different method of interface capturing during the simulation

(b) Time spent for each simulation

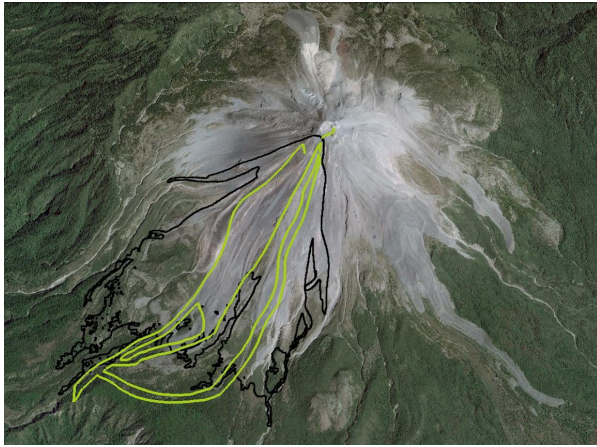
Figure 10: Comparison of the methods based on computational cost

5.2 Colima Volcano

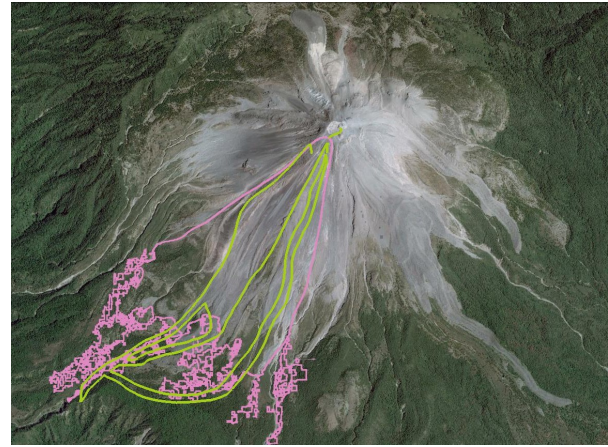
In this section, we verify our different interface capturing methods with a field data of an eruption of Colima volcano. Colima volcano in Mexico is one of the most active volcanoes in North America, and this eruption happened on 16-17 April 1991 [15].

Pile shape	Parabolic
Location of pile in X	644956.0
Location of pile in Y	2157970.0
Maximum pile height	30 m
Major extent of the pile	55 m
Minor extent of the pile	55 m
Bed friction angle	37°
Internal friction angle	20°
Physical time simulated	3600 sec

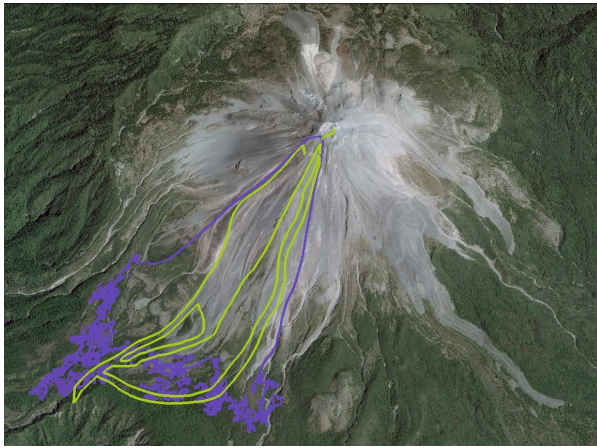
The topography of Colima volcano is such that small changes the initial location of the pile leads to a completely different path of flow, so a good performance of any of the interface capturing methods for this case promises a reliable method for other volcanoes. To be able to compare our results with the outline of deposit of flow, we record the history of all points with the finest resolution of the mesh during the simulation to check the points that are placed exactly on the boundary of the flow. As a definition boundary here means that the points that the flow passed from them, but has not passed one of their neighbors in different directions. For phase field and level set just with recording the maximum absolute value of ϕ we can find these points by plotting $\phi = 0$, this contour produces deposit line of flow during the time. For the heuristic method we recorded the minimum of the pile height during time and plotted the contour of $h = h_{scale} \times GEOFLOW_TINY$, where $h_{scale} = Volume^{\frac{1}{3}}$. The resolution of the digital elevation model (DEM) of Colima volcano that here we used is 5 meter which is the finest DEM that we have ever used for this volcano. The outline of this eruption is available in [35]. In these results, we used Keyhole Markup Language (KML) to plot them on real terrain by using Google earth application 11.



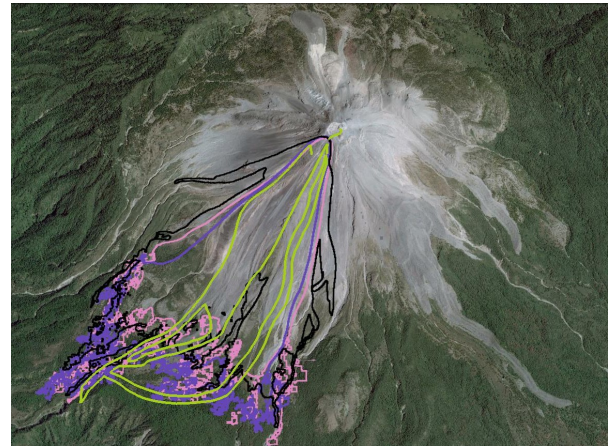
(a) Outline from Heuristic Method



(c) Outline from Phase field Method

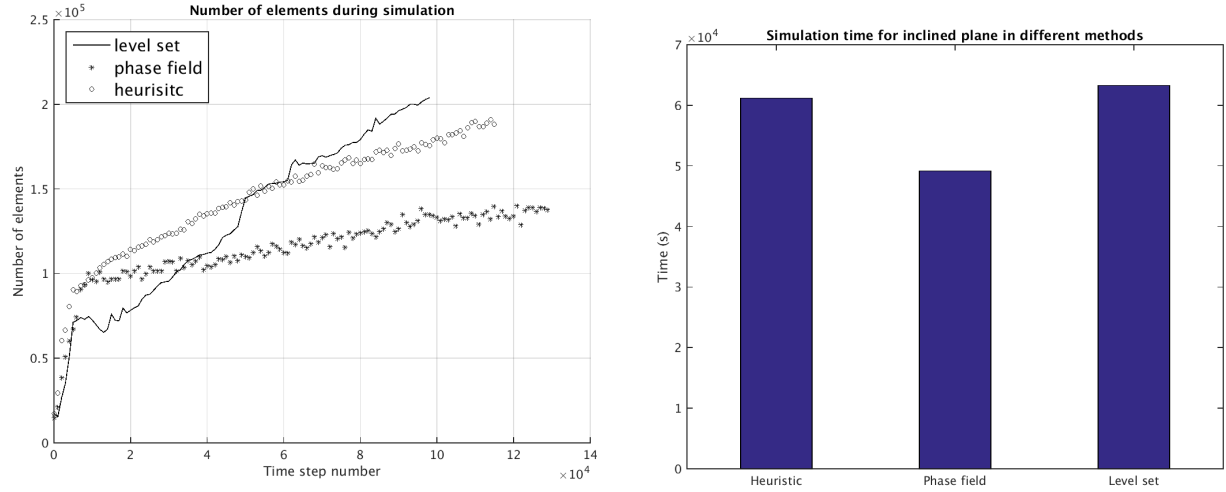


(b) Outline from Level set Method



(d) Comparison of all three methods

Figure 11: Comparison of the obtained outline of flow from Heuristic, Level set, and Phase field methods for Colima Volcano



(a) Number of the elements for different method of interface capturing during the simulation

(b) Time spent for each simulation

Figure 12: Comparison of the methods based on computational cost

6 Conclusions

The numerical solution of the Savage-Hutter (and similar “shallow-water”) equations have historically been plagued by several interrelated numerical difficulties which are collectively characterized by a non-physically thin-layer extending large distances from the realistic main body of the flow. In the best case, this “thin-layer problem” means a “no flow” boundary line must be arbitrarily drawn at some given depth contour. In the worst case, it can cause severe numerical instability that prevents any simulation of a particular event. In this paper, we have described some features of the thin-layer problem, some underlying causes that are common to virtually all numerical solution methodologies. Moreover, we presented a heuristic method and compared two interface capturing approaches that mitigate this problem by addressing its root causes. In heuristic method we used a threshold to distinguish between wet and dry areas, and in the level set and phase field methods we solved a transport equation that implicitly represents the interface of the flow. Then we used the result of previous step for mesh refinement in all of the three solvers to control the thin layer problem and other related problems. Moreover in the heuristic approach we also used this result for interface reconstruction and adjusting the flux. We implemented these thin-layer control strategies in TITAN2D, our high performance finite volume solver of the depth-averaged granular flow equations. Numerical simulations were performed for geophysical mass flows at two different cases. To verify the solvers, numerical experiments were conducted for an inclined plate that finally continues horizontally, and Colima volcano. For the first case we verified the numerical results with experimental results, and for the second case we compared the results with field data. These analysis showed that with all of the approaches, which not only prevented the loss of numerical stability but also demonstrated behavior that is consistent with expectations. On the basis of these very positive results, we concluded that our thin-layer control strategy, and interface capturing approach provides sufficient benefit. While all of these approaches to thin-layer mitigation was developed in the context of TITAN2D’s capabilities, much of it should be appropriate for use in depth-averaged flow solvers with different numerical implementations.

References

- [1] Operators on Inner-Product Spaces. pages 127–161.
- [2] D Adalsteinsson and J.a Sethian. The Fast Construction of Extension Velocities in Level Set Methods. *Journal of Computational Physics*, 148(1):2–22, January 1999.
- [3] a.K. Patra, a.C. Bauer, C.C. Niclita, E.B. Pitman, M.F. Sheridan, M. Bursik, B. Rupp, a. Webber, a.J. Stinton, L.M. Namikawa, and C.S. Renschler. Parallel adaptive numerical simulation of dry avalanches over natural terrain. *Journal of Volcanology and Geothermal Research*, 139(1-2):1–21, January 2005.
- [4] D M Anderson, G B McFadden, and A A Wheeler. Diffuse-Interface Methods in Fluid Mechanics. *Annual Review of Fluid Mechanics*, 30(1):139–165, 1998.
- [5] F. Aureli, a. Maranzoni, P. Mignosa, and C. Ziveri. A weighted surface-depth gradient method for the numerical integration of the 2D shallow water equations with topography. *Advances in Water Resources*, 31(7):962–974, July 2008.
- [6] Satish Balay, Shirang Abhyankar, Mark~F. Adams, Jed Brown, Peter Brune, Kris Buschelman, Victor Eijkhout, William~D. Gropp, Dinesh Kaushik, Matthew~G. Knepley, Lois Curfman McInnes, Karl Rupp, Barry~F. Smith, and Hong Zhang. {PETS}c Users Manual. Technical Report ANL-95/11 - Revision 3.5, Argonne National Laboratory, 2014.
- [7] Andrea Balzano. Evaluation of methods for numerical simulation of wetting and drying in shallow water flow models. *Coastal Engineering*, pages 83–107, 1998.
- [8] W J Boettinger, J a. Warren, C Beckermann, and A. Karma. Phase -Field Simulation of Solidification 1. *Annual Review of Materials Research*, 32(1):163–194, August 2002.
- [9] Lia Bronsard and Robert V Kohn. On the slowness of phase boundary motion in one space dimension. *Communications on Pure and Applied Mathematics*, 43(8):983–997, 1990.
- [10] Shintaro Bunya, Ethan J Kubatko, Joannes J Westerink, and Clint Dawson. A wetting and drying treatment for the Runge–Kutta discontinuous Galerkin solution to the shallow water equations. *Computer Methods in Applied Mechanics and Engineering*, 198(17-20):1548–1562, April 2009.
- [11] John W Cahn. Free Energy of a Nonuniform System. II. Thermodynamic Basis. *The Journal of Chemical Physics*, 30(5), 1959.
- [12] John W Cahn and John E Hilliard. Free Energy of a Nonuniform System. I. Interfacial Free Energy. *The Journal of Chemical Physics*, 28(2), 1958.
- [13] M.J. Castro, A.M. Ferreiro Ferreiro, J.A. García-Rodríguez, J.M. González-Vida, J. Macías, C. Parés, and M. Elena Vázquez-Cendón. The numerical treatment of wet/dry fronts in shallow flows: application to one-layer and two-layer systems. *Mathematical and Computer Modelling*, 42(3-4):419–439, August 2005.
- [14] Vincenzo Casulli. Ahigh-resolution wetting and drying algorithm for free-surface hydrodynamics. *International journal for numerical methods in fluids*, (August 2008):391–408, 2009.
- [15] S J Charbonnier and R Gertisser. Field observations and surface characteristics of pristine block-and-ash flow deposits from the 2006 eruption of Merapi Volcano, Java, Indonesia. *Journal of Volcanology and Geothermal Research*, 177(4):971–982, 2008.
- [16] Long-Qing Chen. {PHASE}-{FIELD} {MODELS} {FOR} {MICROSTRUCTURE} {EVOLUTION}. *Annual Review of Materials Research*, 32(1):113–140, August 2002.

- [17] Liang Cheng and Steven Armfield. A simplified marker and cell method for unsteady flows on non-staggered grids. *International Journal for Numerical Methods in Fluids*, 21(1):15–34, 1995.
- [18] David L. Chopp. Some Improvements of the Fast Marching Method. *SIAM Journal on Scientific Computing*, 23(1):230–244, 2001.
- [19] Keith R Dalbey. PREDICTIVE SIMULATION AND MODEL BASED HAZARD MAPS UMI Number : 3356020 Copyright 2009 by Dalbey , Keith R . All rights reserved. 2009.
- [20] Roger P Denlinger and Richard M Iverson. Flow of variably fluidized granular masses across three-dimensional terrain: 2. Numerical predictions and experimental tests. *Journal of Geophysical Research*, 106(B1):553, 2001.
- [21] L D'Alpaos and a. Defina. Mathematical modeling of tidal hydrodynamics in shallow lagoons: A review of open issues and applications to the Venice lagoon. *Computers & Geosciences*, 33(4):476–496, May 2007.
- [22] M E Eglit and Ye I Sveshnikova. Matematicheskoye modelirovaniye snezhnykh lavin; mathematical modeling of snowavalanches. *Materialy Glyatsiologicheskikh Issledovaniy, Khronika Obsuzhdeniya*, 38:79–84, 1980.
- [23] L Fraccarollo and E F Toro. Experimental and numerical assessment of the shallow water model for two dimensional dam-break type problems. *Journal of Hydraulic Research*, 33:843–864, 1995.
- [24] D Gerlach, G Tomar, G Biswas, and F Durst. Comparison of volume-of-fluid methods for surface tension-dominant two-phase flows. *International Journal of Heat and Mass Transfer*, 49(3-4):740–754, 2006.
- [25] James Glimm, John W Grove, Xiao Lin Li, Keh-Ming Shyue, Yanni Zeng, and Qiang Zhang. Three Dimensional Front Tracking. *SIAM J. Sci. Comp.*, 19:703–727, 1995.
- [26] V R Gopala and B G M van Wachem. Volume of fluid methods for immiscible-fluid and free-surface flows. *Chemical Engineering Journal*, 2008.
- [27] J. M. N. T. Gray, M. Wieland, and K. Hutter. Gravity-driven free surface flow of granular avalanches over complex basal topography. *Proceedings of the Royal Society A: Mathematical, Physical and Engineering Sciences*, 455(1985):1841–1874, May 1999.
- [28] Francis H Harlow and J Eddie Welch. Numerical Calculation of Time-Dependent Viscous Incompressible Flow of Fluid with Free Surface. *Physics of Fluids*, 8:2182–2189, 1965.
- [29] C W HIRT and B D NICHOLS. Volume of fluid/VOF/ method for the dynamics of free boundaries. *Journal of Computational Physics*, 39(1):201–225, 1981.
- [30] R.~M. Iverson. The physics of debris flows. *Reviews of Geophysics*, 35:245–296, 1997.
- [31] Georges Kesserwani and Qiu-hua Liang. Locally Limited and Fully Conserved RKDG2 Shallow Water Solutions with Wetting and Drying. *Journal of Scientific Computing*, 50(1):120–144, March 2011.
- [32] K.Hutter, M Siegel, S B Savage, and Y Nohguchi. Two-dimensional spreading of a granular avalanche down an inclined plane part I. Theory. *Acta Mechanica*, 100:37–68, 1993.
- [33] Junseok Kim. Phase-Field Models for Multi-Component Fluid Flows. *Commun. Comput. Phys*, 12(3):613–661, 2012.
- [34] R G Larson. *The Structure and Rheology of Complex Fluids*. Topics in Chemical Engineering. OUP USA, 1999.

- [35] Laercio M Namikawa. *Multiple Representations of Elevation for Dynamic Process Modeling*. PhD thesis, Department of Geography, University at Buffalo, July 2006.
- [36] Stanley Osher and James A Sethian. Fronts propagating with curvature-dependent speed: Algorithms based on Hamilton-Jacobi formulations. *Journal of Computational Physics*, 79(1):12–49, 1988.
- [37] E B Pitman, A Patra, A Bauer, C Nichita, M Sheridan, and M.Bursik. Computing debris flows. *Physics of Fluids*, 15:3638–3646, 2003.
- [38] S.~P. Pudasaini and K Hutter. Rapid shear flows of dry granular masses down curved and twisted channels. *Journal of Fluid Mechanics*, 495:193–208, November 2003.
- [39] M Quecedo and M Pastor. A reappraisal of Taylor-Galerkin algorithm for drying-wetting areas in shallow water computations. *International Journal for Numerical Methods in Fluids*, 38(6):515–531, 2002.
- [40] S B Savage and K Hutter. The motion of a finite mass of granular material down a rough incline. *Journal of Fluid Mechanics*, 199:177–215, 1989.
- [41] S B Savage and R M Iverson. Surge dynamics coupled to pore-pressure evolution in debris flows. *Debris-Flow Hazards Mitigation: Mechanics, Prediction and Assessment*, edited by: Rickenmann, D. and Chen, C.-L., Millpress, 1:503–514, 2003.
- [42] Mark Sussman, Peter Smereka, and Stanley Osher. A Level Set Approach for Computing Solutions to Incompressible Two-Phase Flow. *Journal of Computational Physics*, 114(1):146–159, 1994.
- [43] Y C Tai, S Noelle, J.M.N.T. Gray, and K Hutter. Shock-Capturing and Front-Tracking Methods for Granular Avalanches. *Journal of Computational Physics*, 175(1):269–301, January 2002.
- [44] Tayfun E Tezduyar, Sunil Sathe, Matthew Schwaab, and Brian S Conklin. Arterial fluid mechanics modeling with the stabilized space – time fluid – structure interaction technique. *International Journal for Numerical Methods in Fluids*, (October 2007):601–629, 2008.
- [45] E F Toro. *Shock-Capturing Methods for Free-Surface Shallow Flows*. Wiley, New York, 2001.
- [46] E F Toro. *Riemann Solvers and Numerical Methods for Fluid Dynamics: A Practical Introduction*. Springer, 2009.
- [47] Salih Ozen Unverdi and Grétar Tryggvason. A Front-tracking Method for Viscous, Incompressible, Multi-fluid Flows. *J. Comput. Phys.*, 100(1):25–37, May 1992.
- [48] Amy Webb. Granular flow experiments to validate numerical flow model, Titan2D, 2004.
- [49] Luiz C Wrobel and C A Brebbia. *Computational Modelling of Free and Moving Boundary Problems: Fluid flow*, volume 1. Walter de Gruyter, 1991.
- [50] Xiaofeng Yang, James J Feng, Chun Liu, and Jie Shen. Numerical simulations of jet pinching-off and drop formation using an energetic variational phase-field method. *Journal of Computational Physics*, 218(1):417–428, 2006.
- [51] D L Youngs. Time-dependent multi-material flow with large fluid distortion. In K W Morton and M J Baines, editors, *Numerical Methods for Fluid Dynamics*, pages 273–285. Academic Press, 1982.